Proceedings of the Institution of Civil Engineers
Water Management 163
November 2010 Issue WM10
Pages 499–507
doi: 10.1680/wama.900024

Paper 900024
Received 17/03/2009
Accepted 05/11/2009

Keywords: river engineering/bridges/hydraulics & hydrodynamics

António H. Cardoso
Professor, Department of Civil Engineering and Architecture, Instituto Superior Técnico, Universidade Técnica de Lisboa, Portugal

Gonzalo Simarro
Associate Professor, Civil Engineering School, Universidad de Castilla – La Mancha, Spain

Olivier Le Doucen
Environmental Engineer, Laboratory of Hydraulic Constructions (LCH), Ecole Polytechnique Fédérale de Lausanne (EPFL), Switzerland

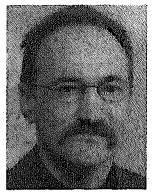

Anton Schleiss
Professor, Laboratory of Hydraulic Constructions (LCH), Ecole Polytechnique Fédérale de Lausanne (EPFL), Switzerland

Sizing of riprap for spill-through abutments

A. H. Cardoso PhD, G. Simarro PhD, O. Le Doucen and A. Schleiss PhD

An experimental investigation of riprap stability at spill-through abutments has been carried out in two similar horizontal-bed flumes, avoiding riprap failure modes other than shear failure and erosion failure. Tests were conducted for two common abutment side slopes, sub-critical flow regime, short to intermediate abutment lengths and high bed roughness. The aim of the experiments was to determine the size of stone riprap necessary to resist (*a*) shear failure in aprons placed at the base of spill-through abutments, and (*b*) erosion failure over their side slopes. Results are compared with predictions of stone riprap size given by expressions found in the literature. The predictor of Pagán–Ortiz is confirmed as being appropriate for shear failure at abutment aprons and can be adapted to account for erosion failure over abutment side slopes. Alternatively, two new expressions, written in terms of the (critical) approach flow intensity required to make the riprap stones move, are suggested.

NOTATION

a, b	coefficients that depend on the abutment side slope
B	width of the flow cross-section
$B_* = L_t/B \equiv L/B$	cross-section contraction
C	coefficient that depends on the type of abutment and its side slope
d	approach flow depth
$D_* = D_{r50}/d$	relative roughness of the riprap blocks
D_{r50}	median size of stable riprap blocks
d_1	flow depth in contracted cross-section
$F_r = U/\sqrt{gd}$	Froude number of the approach flow
$F_{r1} = U_1/\sqrt{gd_1}$	Froude number in contracted cross-section
g	acceleration of gravity
$I_s = U_s/U_c \approx u_{*s}/u_{*c}$	critical flow intensity
I_{s0}	coefficient that depends on the abutment side slope
L	mean (representative) abutment length
L_t	abutment top length
$L_* = L_t/d \equiv L/d$	relative abutment length
s_r	specific gravity of blocks
U	mean approach flow velocity
U_c	critical mean flow velocity of riprap for undisturbed uniform flow
U_s	mean approach flow velocity above which (shear or erosion) failure occurs
U_1	mean flow velocity in contracted cross-section
u_{*c}	critical shear velocity of riprap for undisturbed uniform flow
u_{*s}	shear velocity of approach flow above which shear failure occurs
α	angle of a margin with the horizontal
β	descriptor of the failure area
ρ	water density
ρ_s	density of blocks
σ_D	gradation coefficient of riprap blocks
τ_c	shear stress of approach flow above which erosion failure occurs on the abutment side slope
τ_{c0}	critical shear stress for the initiation of motion of blocks on a undisturbed uniform flat bed flow
ϕ	friction angle of riprap blocks

1. INTRODUCTION

For a long time engineers have made use of riprap as a countermeasure against scour at bridge piers and abutments. Riprap is designed to create a physical barrier intended to resist the erosion capacity of the flow.

The calculation of the median size of stone riprap depends upon an understanding of the riprap failure mechanisms. Riprap placed in a horizontal apron at the base of abutments may be subjected to shear failure, edge failure, winnowing failure and bed-form undermining. Shear failure occurs where the individual riprap stones are not large enough to resist entrainment by the flow; it is clearly linked with the riprap stone size.

According to Melville (Melville *et al.*, 2006a) three failure modes exist for riprap placed on sloping embankments. These are particle erosion failure, translational slide failure and slump failure. Erosion failure, where individual particles are dislodged by the hydrodynamic forces of flowing water, is also strongly linked with the size of the stones.

In the last few years, a number of papers have been published on scour countermeasures for bridge abutments. Most of these were concerned with facing the particular mechanism of edge

failure of riprap aprons or geobags under clear-water or live-bed conditions (e.g. Dey *et al.*, 2008; Korkut *et al.*, 2007; Morales *et al.*, 2008). Studies addressing scour inception (e.g. Kothyari *et al.*, 2007) or riprap failure at spur fields (e.g. Gisonni and Hager, 2008), although not specifically designed as countermeasure studies, also covered the issue of scour countermeasures. However, according to the literature review presented in Section 2, the experimental basis of existing riprap sizing formulations is still limited. Consequently, an experimental investigation of riprap stability at spill-through abutments has been carried out; its results are presented and discussed herein in an attempt to reinforce the existing evidence and knowledge. The aim of the experiments was to determine the size of riprap stones necessary to resist shear failure and erosion failure by the flow, both in aprons placed at the base of spill-through abutments and over their side slopes, guaranteeing that other failure modes are absent. The results are compared with predictions of riprap stone size given by expressions identified in the literature; in addition, new predictors are suggested.

2. LITERATURE REVIEW

Since the 1990s, a few authors have suggested formulations for the evaluation of the median size, D_{r50}, of stable riprap blocks to place at abutment aprons. Such formulations were summarised by Melville and Coleman (2000). For spill-through abutments, those of Pagán-Ortiz (1991) and Richardson and Davis (1995) can be written as

$$\frac{D_{r50}}{d_1} = \frac{C}{s_r - 1} F_{r1}^2 \quad (1)$$

where d_1 is the flow depth in contracted cross-section; s_r is the specific gravity of blocks; $F_{r1} = U_1/\sqrt{gd_1}$ is the Froude number in the contracted cross-section; U_1 is the flow velocity in the contracted cross-section; $C = 0{\cdot}535$ and $0{\cdot}89$ according to Pagán-Ortiz (1991) and Richardson and Davis (1995), respectively, in the range of $F_{r1} < 0{\cdot}8$.

Melville and Coleman (2000) present a diagram in which they predict the domains of occurrence of the four possible failure mechanisms of riprap placed in an apron. The diagram makes use of the ratio u_{*s}/u_{*c}, where u_* is shear velocity, and the subscripts c and s signify 'critical conditions for shear entrainment in undisturbed uniform flow' and 'approach flow conditions leading to shear entrainment at the abutment', respectively. These authors give the approximate value of $u_{*s}/u_{*c} = 0{\cdot}35$ for the riprap entrainment threshold, irrespective of the shape and length of the abutment; this threshold value is also suggested for cylindrical piers.

Melville *et al.* (2006a, 2006b, 2007) focused on the design of riprap aprons to protect spill-through abutments as well as wing-wall abutments for both clear water and live bed conditions. For design purposes for wing-wall abutments, Melville *et al.* (2007) suggest the use of Equation 1 with $C = 1{\cdot}02$ or $0{\cdot}69$, for $F_{r1} < 0{\cdot}8$ or $F_{r1} > 0{\cdot}8$, respectively. No criterion for riprap sizing of spill-through abutment aprons was suggested.

A systematic experimental campaign on the characterisation of block size, mattress thickness and layout of the protected area has recently been carried out by Cardoso and Fael (2009) for vertical-wall abutments, which covered clear-water situations. These authors established the following dependence between the critical flow intensity, I_s, and the relative abutment length, L/d (L = abutment length; d = approach flow depth)

$$I_s = 1 - \frac{2}{5}\left(\frac{L}{d}\right)^{\frac{1}{4}} \quad (2)$$

which stands for $L/d < 9{\cdot}4$ and $d/D_{r50} > 7{\cdot}7$. It should be noted that $I_s = U_s/U_c \approx u_{*s}/u_{*c}$, where U_s is the mean approach flow velocity above which shear failure occurs at the abutment apron and U_c is the critical flow velocity of riprap for undisturbed uniform flow conditions. This means that Equation 2 is, somehow, a generalisation of the criterion of Melville and Coleman (2000) – that is, $I_s \approx u_{*s}/u_{*c} = 0{\cdot}35$.

The experimental basis for the formulation of Pagán-Ortiz (1991) is limited, as pointed out by Melville *et al.* (2007) and the same criticism applies to the contribution of Richardson and Davis (1995) who partly used the data of Pagán-Ortiz (1991). As the remaining known contributions do not directly apply to spill-through abutments, the present study was conceived to further characterise the size of riprap blocks to be placed in aprons at the base of spill-through abutments as a countermeasure against scouring. The study equally addresses the sizing of riprap blocks used in the side slope of abutments.

3. EXPERIMENTAL SET-UP AND PROCEDURE

Two similar horizontal-bed flumes (Figure 1) were used in this study. Both include a central reach containing a recess box in the bed, where the spill-through abutment models were placed, protruding at right angles from one of the vertical side walls. The main features of the flumes are shown in Table 1, where B is the flume width and, according to Figure 1, L_c is the actual flume length, L_u is the distance from the flume entrance to the abutment axis, L_b is the length of the bed recess box and d_b is its depth.

Tests were conducted for abutment side slopes, $H:V$ (see Figure 2), equal to 2 : 1 and 3 : 2. Abutment model height, as measured from the surrounding bed, and top width were, respectively, 130 and 100 mm. Abutments extended downwards vertically from the reference bed level and their bases were directly placed on the bed of the recess boxes; the

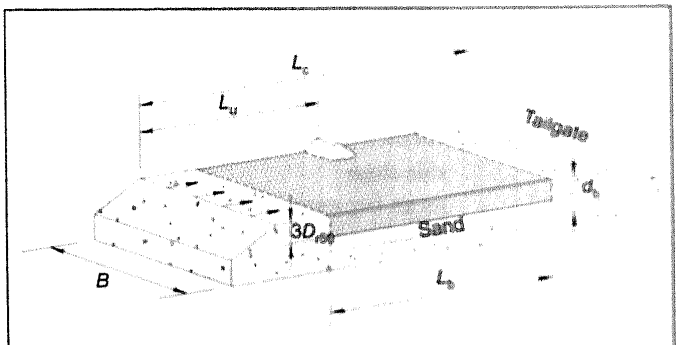

Figure 1. Sketch of the flumes used in the study (not to scale)

Flume	B: m	L_c: m	L_u: m	L_b: m	d_b: m	$H:V$	Riprap			
							Designation	D_{r50}: mm	σ_D	U_c: m/s
UCLM	3·00	7·00	3·60	4·00	0·60	2:1	M1	4·5	1·30	0·62
							M2	7·6	1·19	0·76
							M3	11·9	1·13	0·91
EPFL	1·50	7·10	3·70	3·00	0·30	3:2	L1	4·8	1·15	0·63
							L2	6·9	1·19	0·73

Table 1. Main features of the two flumes and corresponding riprap blocks

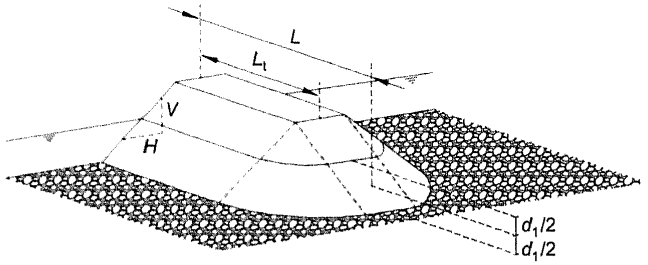

Figure 2. Schematic view of the spill-through abutments

side slopes had a 10 mm thick layer of a modelling compound (Play-doh). This layer made it possible to drive in a new layer of stones which created (*a*) the proper roughness of the abutments' side slopes – during shear failure tests – and (*b*) the 'foundation' where a second layer of loose stones was spilled, prior to each test on erosion failure.

The recess boxes were filled with natural quartz sand. A $3D_{r50}$ thick layer – one for each stone size – of riprap stones was placed on top of the sand such that the upper surface of the riprap was levelled with the adjacent fixed bed of the flume. The upstream reach of the fixed bed was roughened with a loose layer of riprap so as to contribute to the development of the boundary-layer. In all cases, the $3D_{r50}$ riprap layer within the recess box was shown to act as a granular filter with respect to the underlying sand, this way guaranteeing that winnowing failure could not take place; since the recess boxes were entirely covered with riprap, edge failure and bed form undermining were also inhibited.

The tests on shear failure of riprap at aprons involved the replacement of a $1D_{r50}$ thick layer of riprap by yellow painted stones of the same size (see Figure 3(a)) in the zone where shear failure was expected – and confirmed – to occur. Tests started with very low flow velocities. The velocity was successively increased, while the flow depth was maintained constant in the range 0·09 m $\leq d_1 \leq$ 0·12 m, by increasing the discharge and adjusting the downstream tailgate, which means that abutments were never submerged. This procedure was continued until the riprap stones close to the abutment began to move. A typical bed at the end of tests is shown in Figure 3(b). The beginning of motion is difficult to identify in the laboratory because of its stochastic nature resulting in its visual evaluation being somewhat subjective. Hence, two approximate values of U_s were recorded: a lower one, where

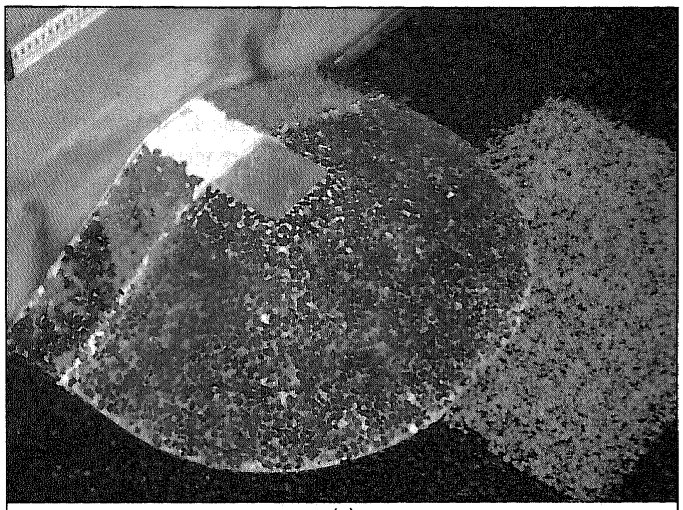

(a)

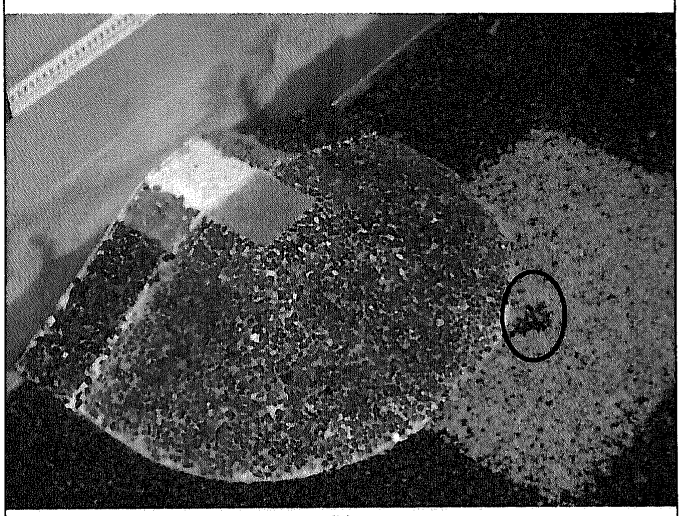

(b)

Figure 3. Abutment and surrounding: (*a*) bed before the shear failure test; (*b*) after the shear failure test

motion was about to take place but had not yet been observed – isolated stones were observed to tremble but did not leave their positions – and an upper one, corresponding to very weak sediment motion (incipient motion). The velocity intervals were very small though certainly containing the true U_s value.

Fourteen shear failure tests were carried out in flume UCLM ($B = 3$ m) for $H:V = 2:1$, corresponding to abutment top lengths (see Figure 2), L_t = 0·10, 0·20, 0·30, 0·40, 0·50 and 0·60 m. For each length, at least two riprap block sizes, M1 and M2 in Table 1, were tested; for L_t = 0·40 and 0·50 m, block size

M3 was tested too. The characteristics of riprap mixtures, namely the median diameter of the stone size distribution, D_{r50}, and the associated gradation coefficient, σ_D, are indicated in Table 1. Riprap size distributions can be considered uniform since $\sigma_D < 1{\cdot}5$. Shape factor and angularity were not measured but, on the basis of the authors' experience, stones were angular to very angular and their shape factor was around 0·7–0·8.

At the end of each shear failure test, the bed was relevelled and the side slopes of the abutment were partly covered with an approximately $1D_{r50}$ thick layer of riprap stones which imbricate on a layer of stones previously embedded in the 10 mm thick layer of modelling compound (Play-doh), Figure 4(a). The resulting configuration was stable for both dry and underwater conditions, which means that translational slide failures and slump failures were absent. The same experimental procedure as described for the shear failure tests was then adopted but based on a few riprap stones being dislodged from the side slope of the abutment (Figure 4(b)), as the way of identifying critical particle erosion failure. Fourteen particle erosion tests were performed, one per shear failure test. As erosion failure occurred for flow velocities that were smaller than the corresponding shear failure velocities, the bed surrounding the abutment remained undisturbed in all cases.

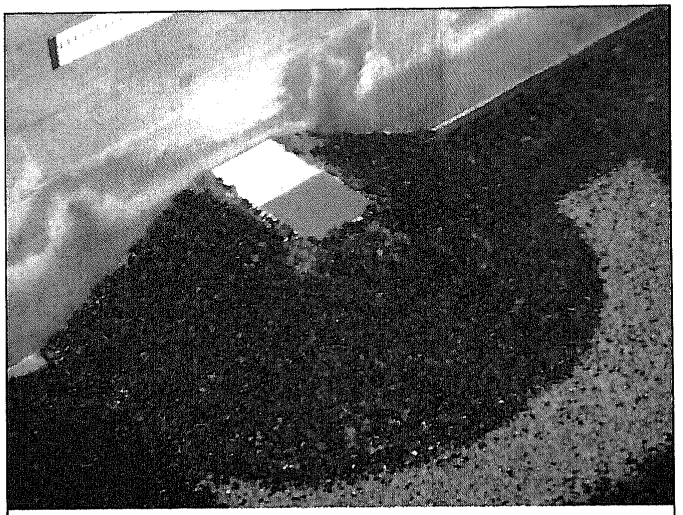

(a)

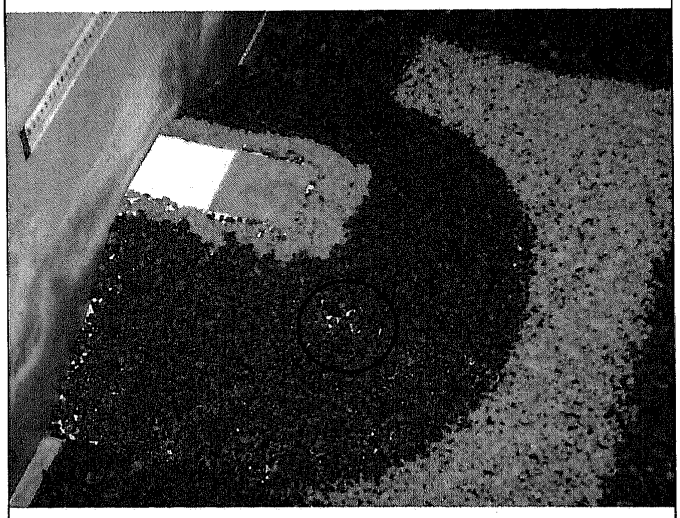

(b)

Figure 4. Abutment and its side slope cover: (*a*) before the particle erosion test; (*b*) after the particle erosion test

Similarly, six shear failure tests were carried out in the flume EPFL ($B = 1{\cdot}5$ m) for $H : V = 3 : 2$, corresponding to abutment top length, $L_t = 0{\cdot}10$, 0·20 and 0·30 m. Two different riprap stones – L1 and L2 in Table 1 – were tested. An equal number of particle erosion tests were performed in the same facility.

It should be noted that the ratio L/B, where L is the mean (representative) abutment length (Figure 2), was limited to approximately 0·2 in both flumes. For this range of L/B, the flow depths immediately upstream of the abutment and at the contracted cross-section were practically equal. Consequently, the water level difference was measured at approximately 1·0 m upstream of the abutment axis and is assignable to both the approach flow and the contracted cross-section.

Two complementary tests were carried out to characterise the critical velocity of initiation of motion of riprap blocks M1 and M2 under the undisturbed, uniform flow conditions. The observed values of U_c were verified to be practically equal to the predictions of the Neil (1967) and Garde (1970) equations. The average of the values predicted by these equations was, thus, adopted in the present study and recorded in Table 1 as U_c.

4. RESULTS AND DISCUSSION

4.1. Shear failure at abutment aprons

The results of the 20 tests carried out on shear failure at abutment aprons are summarised in Table 2. In this table, test Lt10D8a, for instance, is the test where $L_t = 10$ cm and $D_{r50} \approx 8$ mm, and 'a' signifies 'at the apron' around the abutment; this mnemonic applies to all shear failure tests; U_{min} is the velocity limit at the contracted cross-section where sediment motion is about to take place but has not yet been observed; U_{max} is a velocity at the same cross-section corresponding to very weak sediment motion (incipient shear failure); F_{r1} is calculated with the average of U_{min} and U_{max} and I_s is calculated with the average of the corresponding approach flow values.

Bearing in mind the structure of Equation 1, the values of D_{r50}/d_1 are plotted against Froude number, F_{r1}, in Figure 5. This figure also includes the results derived from Equation 1 for the constants C suggested by Pagán-Ortiz (1991) and Richardson and Davis (1995). It can be concluded that, within the experimental range of the present study, the predictor of Pagán-Ortiz provided an excellent upper envelope curve to the data, whereas the predictor of Richardson and Davis seemed to over-size riprap stones at abutment aprons.

Figure 6 shows the comparison between experimental results for I_s and those predicted according to Hager and Oliveto (2002). Their expression seems to fall on the unsafe side, leading to values of the mean approach flow velocity above which greater shear failure than the observed events occurs. It should be noted that the equation of Hager and Oliveto for the inception velocity relies on the contraction provoked by the abutment as independent parameter. Thus, their expression is apparently meant for cases in which contraction dominates the local scour phenomenon, but not for cases in which the contraction effects are of minor importance.

In many practical circumstances, it is convenient to make

Test	$H:V$	D_{r50}: mm	d_1: m	L: m	U_{min}: m/s	U_{max}: m/s	F_{r1}	D_{r50}/d_1	L/d_1	l_s
Lt10D4a	2 : 1	4·5	0·097	0·263	0·369	0·383	0·42	0·046	2·71	0·61
Lt20D4a			0·096	0·364	0·346	0·359	0·41	0·047	3·78	0·57
Lt30D4a			0·099	0·461	0·336	0·343	0·41	0·045	4·64	0·55
Lt40D4a			0·096	0·564	0·316	0·326	0·41	0·047	5·85	0·52
Lt50D4a			0·098	0·662	0·287	0·296	0·38	0·046	6·73	0·47
Lt60D4a			0·097	0·763	0·294	0·301	0·41	0·046	7·83	0·48
Lt10D8a	2 : 1	7·6	0·103	0·257	0·487	0·502	0·54	0·074	2·51	0·65
Lt20D8a			0·101	0·359	0·436	0·465	0·51	0·075	3·56	0·59
Lt30D8a			0·111	0·449	0·424	0·437	0·49	0·069	4·06	0·57
Lt40D8a			0·108	0·552	0·406	0·420	0·49	0·070	5·10	0·54
Lt50D8a			0·105	0·655	0·366	0·379	0·47	0·073	6·24	0·49
Lt60D8a			0·104	0·756	0·352	0·364	0·47	0·073	7·27	0·47
Lt40D12a	2 : 1	11·9	0·117	0·543	0·481	0·495	0·56	0·101	4·63	0·54
Lt50D12a			0·118	0·642	0·477	0·491	0·57	0·100	5·43	0·53
Lt10D5a	3 : 2	4·8	0·090	0·295	0·356	0·370	0·48	0·053	3·28	0·57
Lt20D5a			0·090	0·395	0·319	0·333	0·47	0·053	4·39	0·52
Lt30D5a			0·090	0·495	0·274	0·289	0·45	0·053	5·50	0·44
Lt10D7a	3 : 2	6·9	0·090	0·295	0·393	0·415	0·54	0·077	3·28	0·55
Lt20D7a			0·090	0·395	0·356	0·378	0·53	0·077	4·39	0·50
Lt30D7a			0·090	0·495	0·311	0·326	0·51	0·077	5·50	0·44

Table 2. Results of shear failure tests at aprons of spill-through abutments

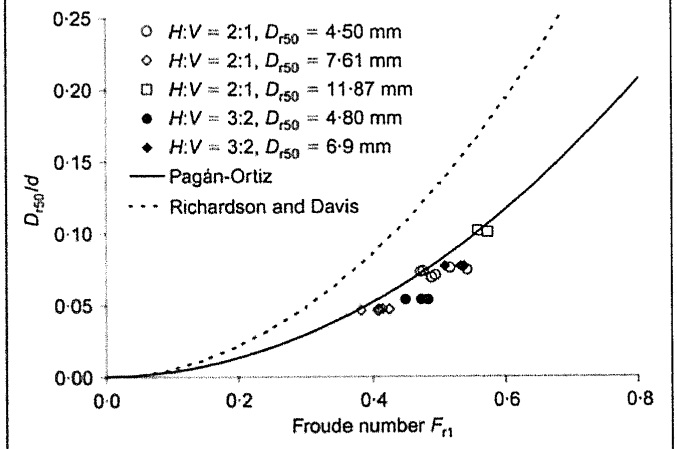

Figure 5. Variation of critical apron shear failure D_{r50}/d_1 with the Froude number, F_{r1}, of the contracted cross-section

predictions on the basis of the approach flow variables. In that case, the relative abutment length plays a paramount role, as implied by Equation 2 of Cardoso and Fael (2009). The data of critical shear failure at the abutment aprons is presented in Figure 7 by using the approach flow variables. This figure shows that, for a given stone size (or U_c) and a given flow depth, the approach flow velocity that induces shear failure, U_s, decreases with the abutment length. This variation comes as no surprise since the longer the abutment, the greater the discharge diverted to the abutment's nose and, consequently, the greater the local flow velocity and the propensity for failure. Note that the abutment length is normalised with the water depth. For the sake of comparison, the figure includes the envelope curve suggested by Cardoso and Fael (2009) for vertical wall abutments. The three envelope curves, one per side slope, can be written in the following unified form

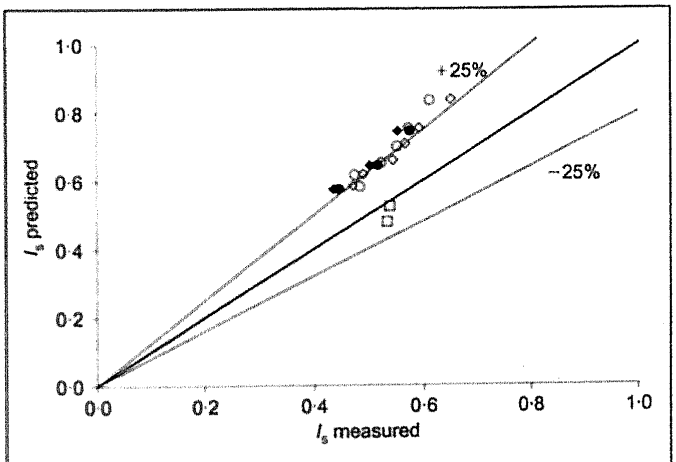

Figure 6. Critical apron shear failure flow intensity l_s: experimental data plotted against predictions of Hager and Oliveto's expression

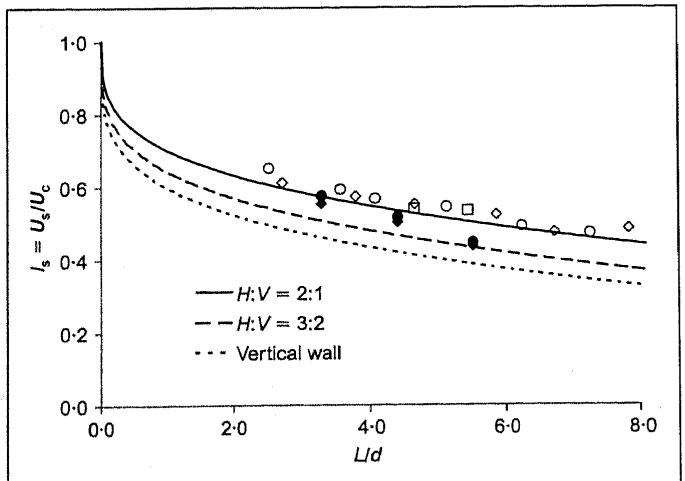

Figure 7. Variation of critical apron shear failure flow intensity l_s with L/d. Open symbols correspond to $H:V = 2:1$; black symbols correspond to $H:V = 3:2$ (legend of Figure 5 remains valid)

$$3 \qquad I_s = 1 - a\left(\frac{L}{d}\right)^b$$

Equation 3 inherently assumes that the approach flow depth, d, and the contracted cross-section flow depth, d_1, are equal; and both a and b depend on the abutment side slope. This dependence was established in the present study as indicated in Table 3 and plotted in Figure 8.

Abutment type	a	b
Vertical wall	0·400	0·250
Spill-through, $H:V = 3:2$	0·355	0·275
Spill-through, $H:V = 2:1$	0·300	0·300

Table 3. Values of a and b of Equation 3 for different abutment side slopes

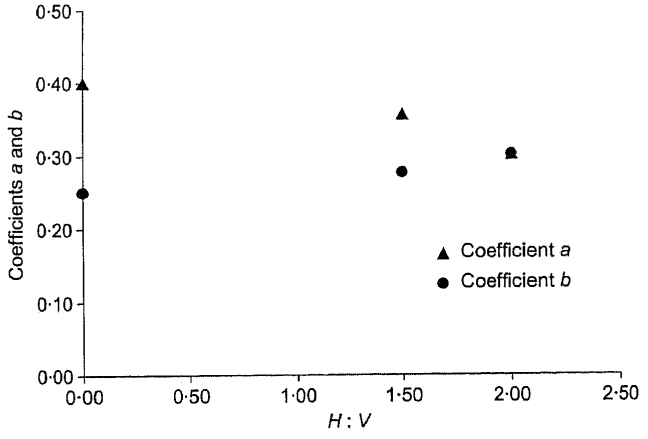

Figure 8. Coefficients a and b as a function of abutment slope $H:V$

In summary, Equation 1 with $C = 0{\cdot}535$, as suggested by Pagán-Ortiz (1991), seems a good predictor of D_{r50}; as an alternative, Equation 3 with constants a and b as given in Table 3 for different slopes may be used. It should, however, be noticed here that these conclusions are valid within the experimental range of this study ($9{\cdot}9 < d_1/D_{r50} < 22$; $L/d_1 < 7{\cdot}8$; $F_{r1} < 0{\cdot}57$), with special emphasis on the fact that L/B must be smaller than 0·2.

4.2. Erosion failure at abutment side slopes

The results of erosion failure tests at the abutment side slopes are summarised in Table 4. In this table, the mnemonic of Table 2 remains valid with 's' signifying 'at the side slope' of the abutment. The meaning of the other variables is also the same.

Referring again to Equation 1, the values of D_{r50}/d_1 for the erosion failure tests are plotted against F_{r1} in Figure 9. The

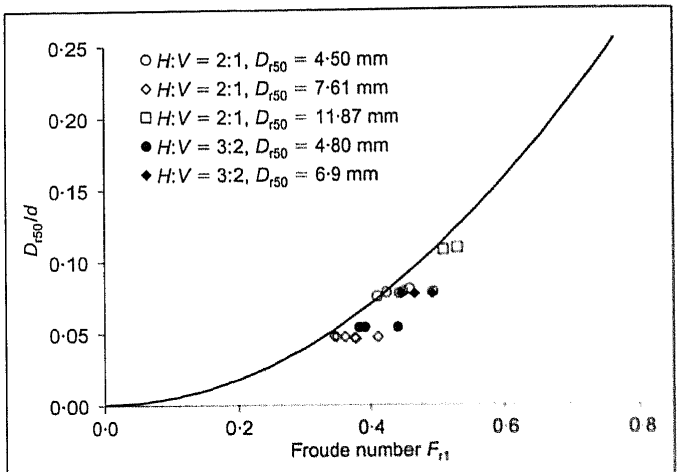

Figure 9. Variation of critical side slope erosion failure D_{r50}/d_1 with the Froude number of the contracted cross-section, F_{r1}. The solid line corresponds to the expression of Pagán-Ortiz but considering $C = 0{\cdot}720$

Test	$H:V$	D_{r50}: mm	d_1: m	L: m	U_{min}: m/s	U_{max}: m/s	F_{r1}	D_{r50}/d_1	L/d_1	I_s
Lt10D4s	2 : 1	4·5	0·097	0·263	0·358	0·371	0·41	0·047	2·73	0·59
Lt20D4s			0·098	0·362	0·371	0·329	0·38	0·046	3·71	0·52
Lt30D4s			0·099	0·461	0·302	0·326	0·38	0·046	4·68	0·51
Lt40D4s			0·096	0·564	0·282	0·287	0·36	0·047	5·87	0·46
Lt50D4s			0·096	0·664	0·261	0·265	0·35	0·047	6·91	0·43
Lt60D4s			0·096	0·764	0·245	0·251	0·34	0·047	7·99	0·40
Lt10D8s	2 : 1	7·6	0·098	0·262	0·434	0·449	0·49	0·078	2·68	0·58
Lt20D8s			0·098	0·362	0·367	0·407	0·45	0·078	3·71	0·51
Lt30D8s			0·095	0·465	0·362	0·389	0·46	0·080	4·87	0·49
Lt40D8s			0·099	0·561	0·349	0·362	0·44	0·077	5·67	0·47
Lt50D8s			0·102	0·658	0·316	0·323	0·41	0·075	6·47	0·42
Lt60D8s			0·098	0·762	0·304	0·316	0·42	0·078	7·77	0·41
Lt40D12s	2 : 1	11·9	0·109	0·551	0·442	0·456	0·53	0·108	5·03	0·49
Lt50D12s			0·111	0·649	0·410	0·423	0·51	0·107	5·86	0·46
Lt10D5s	3 : 2	4·8	0·090	0·295	0·326	0·341	0·44	0·053	3·28	0·53
Lt20D5s			0·090	0·395	0·259	0·281	0·39	0·053	4·38	0·43
Lt30D5s			0·090	0·495	0·230	0·252	0·38	0·053	5·50	0·38
Lt10D7s	3 :2	6·9	0·090	0·295	0·341	0·363	0·47	0·077	3·28	0·48
Lt20D7s			0·090	0·395	0·333	0·348	0·49	0·077	4·39	0·47
Lt30D7s			0·090	0·495	0·274	0·289	0·45	0·077	5·50	0·38

Table 4. Results of erosion failure tests at the side slope of spill-through abutments

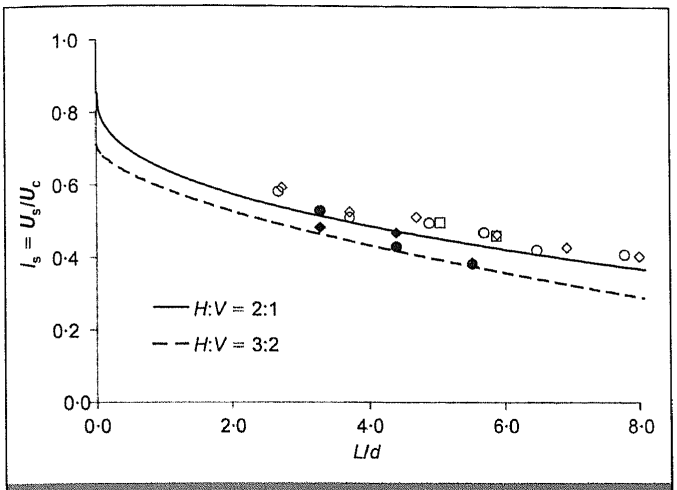

Figure 10. Variation of critical side slope erosion failure flow intensity I_s with L/d. Open symbols correspond to $H:V = 2:1$; black symbols correspond to $H:V = 3:2$ (legend of Figure 5 remains valid)

Abutment type	a	b	I_{s0}
Spill-through, $H:V = 3:2$	0·12	0·60	0·71
Spill-through, $H:V = 2:1$	0·21	0·40	0·85

Table 5. Values of a, b and I_{s0} of Equation 4 for different abutment side slopes

general trend of failure is similar to the one shown in Figure 5 for shear, as expected, but failure occurs for smaller contracted flow velocities, however. Equation 1 was adapted as an envelop curve, with C having a value of 0·720, to reflect the greater propensity for failure at side slopes than at horizontal aprons. This compares with the value of C of 0·535, proposed by Pagán-Ortiz (1991).

The erosion failure results were also analysed in the framework of Equation 3, as generalised to

$$I_s = I_{s0} - a\left(\frac{L}{d}\right)^b \quad (4)$$

where I_{s0} is a parameter that depends on the abutment slope. According to Figure 10, Equation 4 constitutes an excellent lower envelope curve for the erosion failure data, with the values of I_{s0}, a and b as recorded in Table 5.

Equation 2 of Cardoso and Fael (2009) was established for aprons at the base of vertical-wall abutments. For $L = 0$, the flat bed shear failure condition is recovered from Equation 2; that is, U_s becomes equal to U_c. In the case of erosion on side slopes, the equivalent condition of initiation of motion of particles on the sloped margins must also be recovered for $L = 0$. This is the reason why the constant '1' of Equations 2 and 3 was replaced by I_{s0} in Equation 4.

The value of I_{s0} can be estimated analytically for a given slope. The critical shear stress, τ_c, for the initiation of motion of a given block on a sloped margin is given by (e.g. Graf and Altinakar, 1998)

$$\tau_c = \tau_{c0}\cos\alpha\sqrt{1 - \frac{\tan^2\alpha}{\tan^2\phi}} \quad (5)$$

where τ_{c0} is the critical shear stress for the same block in the flat bed case, α is the angle of the margin to the horizontal, and ϕ is the friction angle of the blocks. The value of I_s corresponding to $L = 0$; that is, I_{s0} is the ratio of the mean velocity required to move the blocks on the margin, U_s, to the mean velocity required to move them on a horizontal bed, U_c. Recalling Equation 5, and as τ is proportional to U^2, then I_{s0} is given by

$$I_{s0} = \sqrt{\cos\alpha\sqrt{1 - \frac{\tan^2\alpha}{\tan^2\phi}}} \quad (6)$$

Assuming the friction angle of the tested blocks to be $\phi \approx 40°$, I_{s0} becomes $I_{s0} \approx 0{\cdot}85$ for $H:V = 2:1$ and $I_{s0} \approx 0{\cdot}71$ for $H:V = 3:2$, which correspond to the values shown in Table 5. Naturally, the steeper the slope, the lower the I_{s0} value.

5. FURTHER DISCUSSION

The minimum size of stable riprap blocks, D_{r50}, is a function of the block density, ρ_s, the water density, ρ, the approach flow depth, d, and mean velocity, U, the gravity, g, and geometry of the problem: basically, the slope angle α (i.e. $H:V$), the top length of the abutment, L_t, the channel width, B, and the zone under consideration (apron or side slope). Thus, dimensional analysis yields

$$D_* = f(s_r, Fr, L_*, B_*, s_r, \alpha, \beta) \quad (7)$$

where $s_r = \rho_s/\rho$ = specific gravity of blocks, β means apron (i.e. $\beta = a$) or side slope ($\beta = s$), and

$$D_* = \frac{D_{r50}}{d}, \quad Fr = \frac{U}{\sqrt{gd}}, \quad L_* = \frac{L_t}{d}, \quad B_* = \frac{L_t}{B} \quad (8)$$

are other dimensionless groups. It should be noted here that the approach flow variables U and d can consistently be replaced by those of the contracted cross-section, U_1 and d_1, somehow introducing geometric effects into the Froude number. Also, L_t can be replaced by L and hereafter B_* will stand for L/B. It should also be noted that Equation 1 of Pagán-Ortiz (1991), which makes use of the contracted cross-section variables, is a particular case of Equation 7. The absence of dimensionless groups L_*, B_*, α and β in Equation 1 may be explained using two different forms of reasoning: (*a*) some groups are of marginal interest to the analysis (e.g. B_* when $B_* << 1$ and contraction effects are negligible); and (*b*) some others were assumed to be constant (e.g. specific gravity of the blocks or geometric parameters). In these circumstances, F_{r1} turns out to become the proper representative dimensionless group of the phenomenon. Further, since the flow regime is rough turbulent, it can be shown, according to Simarro *et al.* (2007) that

$$Fr = 0{\cdot}75I\sqrt{D}\ln\frac{11}{D_*} = f(D_*, I) \quad (9)$$

where $I = U/U_c$. Thus, assuming, as usual, that the specific gravity, s_r, is constant, Equation 7 is also $D_* = f(I, L_*, B_*, \alpha, \beta)$ or, conversely, looking for the critical mean velocity, U_s, of a given block size

$$I_s = f(D_*, L_*, B_*, \alpha, \beta) \quad (10)$$

The value of $I_s \approx 0{\cdot}35$ as given by Melville and Coleman (2000) can now be seen as a particular case of Equation 10. The absence of D_* can be explained by the use of flow intensity which, according to Equation 9, incorporates the effect of block size; the absence of the variable L_* is harder to explain, unless only a small range of L_* has been covered. Equation 2 of Cardoso and Fael (2009) as well as its generalisation into Equation 4 are also expressions of Equation 10, which include L_* and other geometric characteristics.

As emphasised above, this study is restricted to small values of B_*, namely to situations in which the contraction effects are negligible. One of the consequences of this restriction is that $d \approx d_1$; also, B_* does not appear in Equations 3 and 4. However, for large values of B_*, the influence of this parameter is expected to be strong, as, in the absence of a scour hole to convey the flow intercepted by the abutment, the flow is necessarily accelerated in the contracted cross-section, particularly close to the abutment head. Four preliminary tests have been carried out in the flume EPFL for $B_* > 0{\cdot}2$; two of these tests focused on shear failure; the other two focused on erosion failure. It became obvious that neither the predictor of Pagán-Ortiz (1991) nor the new predictors expressed by Figures 7 and 10 or Equations 3 and 4 remain valid for $B_* > 0{\cdot}2$; they under-predict D_{r50} and this must be strongly emphasised.

6. CONCLUSIONS

The use of riprap protection for spill-through abutments under clear-water flow conditions was addressed in this study. Experiments were carried out in which abutments protruded at right angles from the wall of two rectangular sand bed channels. For the experimental range of this study ($9{\cdot}9 < d_1/D_{r50} < 22$; $L/d_1 < 7{\cdot}8$; $F_{r1} < 0{\cdot}57$, $L/B < 0{\cdot}2$; $3{:}2 \leqslant H : V \leqslant 2 : 1$; $B_* < 0{\cdot}2$), the following conclusions can be drawn.

(*a*) The riprap stone sizes required to prevent shear failure at abutment aprons can be properly predicted through the equation of Pagán-Ortiz (1991) with $C = 0{\cdot}535$, exactly as suggested by the author.
(*b*) The same type of equation can be used to size stone riprap capable of preventing erosion failure over the abutment side slopes by increasing the value of the parameter C to 0·72, which reflects the higher propensity of failure on side slopes than on horizontal aprons.
(*c*) The equation of Pagán-Ortiz (1991) makes use of the Froude number in the contracted cross-section as the only independent parameter. Alternatively, the concept of critical approach flow intensity for scour inception can be adopted, supported by a proper dimensional analysis and clearly shown to depend on the ratio of the abutment length to the flow depth.
(*d*) Equations 3 and 4, which make use of critical approach flow intensity, are suggested for practical application.

ACKNOWLEDGEMENTS

The experimental study reported in the paper was partly carried out by the first author during his sabbatical leave at the Ecole Polytechnique Fédérale de Lausanne and at the Universidad de Castilla-la Mancha. He wishes to acknowledge the availability and use of the experimental facilities and the financial support received from those institutions as well as from the Instituto Superior Técnico and the National Science Foundation of Portugal. The authors would also like to thank Eduardo Díaz for his help in preparing the UCLM experiments.

REFERENCES

Cardoso AH and Fael CMS (2009) Protecting vertical-wall abutments with riprap mattresses. *Journal of Hydraulic Engineering* 135(6): 457–465.

Dey S, Chiew YM and Kadam MS (2008) Local scour and riprap stability at an abutment in a degrading bed. *Journal of Hydraulic Engineering* 134(10): 1496–1502.

Garde RJ (1970) Initiation of motion on a hydrodynamically rough surface. Critical velocity approach. *Journal of Irrigation and Power* 6(2)

Gisonni C and Hager WH (2008) Spur failure in river engineering. *Journal of Hydraulic Engineering* 134(2): 135–145.

Graf WH and Altinakar MS (1998) *Fluvial Hydraulics*. Wiley, London, UK.

Hager WH and Oliveto G (2002) Shields' entraintment criterion in bridge piers. *Journal of Hydraulic Engineering* 128(5): 538–542.

Korkut R, Martinez EJ, Morales R, Ettema R and Barkdoll B (2007) Geobag performance as scour countermeasure for bridge abutments. *Journal of Hydraulic Engineering* 133(4): 431–439.

Kothyari UC, Hager WH and Oliveto G (2007) Generalised approach for clear-water scour at bridge foundation elements. *Journal of Hydraulic Engineering* 133(11): 1229–1240.

Melville B and Coleman E (2000) *Bridge Scour*. Water Resources Publications. LLC, Fort Collins, CO, USA.

Melville B, Ballegooy S, Coleman S and Barkdoll B (2006a) Countermeasure toe protection at spill-through abutments. *Journal of Hydraulic Engineering* 132(3): 235–245.

Melville B, Ballegooy S, Coleman S and Barkdoll B (2006b) Scour countermeasures for wing-wall abutments. *Journal of Hydraulic Engineering* 132(6): 563–574.

Melville B, Ballegooy S, Coleman S and Barkdoll B (2007) Riprap size selection at wing-wall abutments. *Journal of Hydraulic Engineering* 133(11): 1265–1269.

Morales R, Ettema R and Barkdoll B (2008) Large-scale flume tests of riprap-apron performance at a bridge abutment on a floodplain. *Journal of Hydraulic Engineering* 134(6): 800–809.

Neil CR (1967) Mean velocity criterion for scour of coarse uniform bed-material. *Proceedings of the XII IAHR Congress*. Fort Collins, CO, USA, pp. 46–54.

Pagán-Ortiz JE (1991) *Stability of Rock Riprap for Protection at the Toe Abutments Located at the Floodplain*. Federal Highway Administration, Department of Transportation, Washington, Report No. FHWA-RD-91-057: 125.

Richardson EV and Davis SR (1995) *Evaluating Scour at Bridges*. US Department of Transportation, Washington, Hydraulic Engineering Circular No. 18 (HEC-18), Report No. FHWA-IP-90-017: 204.

Simarro G, Teixeira L and Cardoso AH (2007) Flow intensity parameter in pier scour experiments. *Journal of Hydraulic Engineering* **133(11)**: 1261–1264.